Modeling and Characterization of Texture Evolution in Twist Extrusion

MARAT I. LATYPOV, MYOUNG-GYU LEE, YAN BEYGELZIMER, DENIS PRILEPO, YURI GUSAR, and HYOUNG SEOP KIM

Twist extrusion (TE) is a severe plastic deformation method with a potential for commercialization. Deformation during the TE process is non-uniform and non-monotonic, which is expected to result in significant and non-trivial microstructural changes in metallic materials. In this study, texture evolution during TE of pre-textured copper was investigated. Experimental characterization of textures after various numbers of passes demonstrated that TE can be used for producing uniformly weak textures in pre-textured copper. Crystal plasticity simulations were found to run into the problem known as strain reversal texture. In particular, crystal plasticity simulations predicted the return of initial texture upon strain reversal in the first pass of TE, whereas the experimental texture was not reversed and had components related to simple shear. Grain refinement, imperfect strain reversal, and material asymmetry are proposed to be responsible for the occurrence of strain reversal texture in TE. Effects of the non-random initial texture on the microstructure and texture evolution are also discussed.

DOI: 10.1007/s11661-015-3298-1

I. INTRODUCTION

SEVERE plastic deformation (SPD) methods are powerful for improving properties of metallic materials yet difficult for commercialization. Twist extrusion (TE) is a promising SPD technique for commercial use. The promise for scale-up ensues from a relatively good compatibility of the process with conventional metal forming techniques, feasibility for processing of large samples, and other practical advantages, such as unidirectional loads,[1] multi-pass processing without reinserting the sample.

In the TE process, a sample of quite an arbitrary cross section is pressed through a die consisting of two straight channels and a so-called twist channel between them[2] (Figure 1(a)). Ideally little change in the cross-sectional shape of the sample allows for repeating the TE process and accumulating large plastic strains. In the first approximation, deformation in TE is simple shear concentrated on two planes where the twist channel intersects the straight channels (highlighted in Figure 1(a)).[2,3] The sense of simple shear acting on the second plane is opposite to that of the first shear, whereas the magnitudes of both shear strains are ideally identical.

Significant changes in the microstructure, crystallographic texture, and thus mechanical properties of metallic materials are expected to occur in response to large strains and marked strain path changes involved in TE. While the evolution of microstructures and mechanical properties was documented and understood to some extent, texture development in TE has received little attention. Indeed, only a few studies[4–8] confined to experimental measurements of TE textures are available to date and are insufficient for a systematic understanding. It is unfortunate because texture is known to have a strong influence on the anisotropy of mechanical and physical properties of the polycrystalline materials. Therefore, knowledge on deformation texture developed as a result of TE would allow for prediction of the behavior of the material during further processing or actual service in structures. Furthermore, understanding of the relationship between texture evolution and the process variables (*e.g.,* die geometry and pass number) would help optimizing the process towards desired properties of the processed material. Finally, investigation of texture and related phenomena in TE are also of scientific interest because complex deformation with large strains and strain path changes is involved in the process.

For these reasons, the current study seeks to advance our knowledge and understanding of texture evolution

MARAT I. LATYPOV, Researcher, formerly with the Center for Advanced Aerospace Materials, POSTECH, Pohang 790-784, Republic of Korea, is now with the Georgia Tech-CNRS UMI 2958, Georgia Tech Lorraine, Metz, France. MYOUNG-GYU LEE, Associate Professor, is with the Department of Materials Science and Engineering, Korea University, Seoul 136-701, Republic of Korea. YAN BEYGELZIMER, Professor, is with the Donetsk Institute of Physics & Engineering Institute of the National Academy of Sciences of Ukraine (NAS), Kyiv 03028, Ukraine, and also with the Laboratory of Excellence on Design of Alloy Metals for Low-Mass Structures (DAMAS), Université de Lorraine, Metz 57000, France. DENIS PRILEPO and YURI GUSAR, Researchers, are with the Donetsk Institute of Physics & Engineering of the National Academy of Sciences of Ukraine (NAS). HYOUNG SEOP KIM, Professor, is with the Center for Advanced Aerospace Materials, POSTECH, and also with the Department of Materials Science and Engineering, POSTECH. Contact e-mail: hskim@postech.ac.kr

Marat I. Latypov and Myoung-Gyu Lee have contributed equally to the present work.

Manuscript submitted June 18, 2015.
Article published online December 30, 2015

in TE. One of the objectives of the present paper was to document texture evolution in multi-pass TE of an fcc metal. This objective was accomplished through X-ray diffraction measurements of textures in copper after various numbers of passes. Another goal of the present study was to understand *how* texture develops during the TE process, for which finite-element modeling and crystal plasticity simulations were performed for one TE pass. With acknowledgement of non-uniform deformation in TE, attention was paid to possible spatial variations of texture in both modeling and characterization.

II. EXPERIMENTAL AND MODELING PROCEDURES

A. *Material and Processing by Twist Extrusion*

Commercially pure copper M1 (99.9 pct, see Table I) in an as-received state was used for the present study. The copper was received in rods with a diameter of 50 mm produced by hot pressing in Artemovsk Works (Ukraine). For processing by TE, samples of a length of 70 mm were machined from the as-received rods. The samples measured 28 $\times$ 18 mm in cross section and had a rectangular shape with two arc sides (Figure 1). A TE die with a 90 deg clockwise twist (*i.e.*, angle χ) was used for processing. The TE process was conducted at a temperature of ~340 K (~65 °C) with a ram speed of 3 mm/s. Back pressure of a magnitude of 250 MPa was applied to the leading end of the sample.

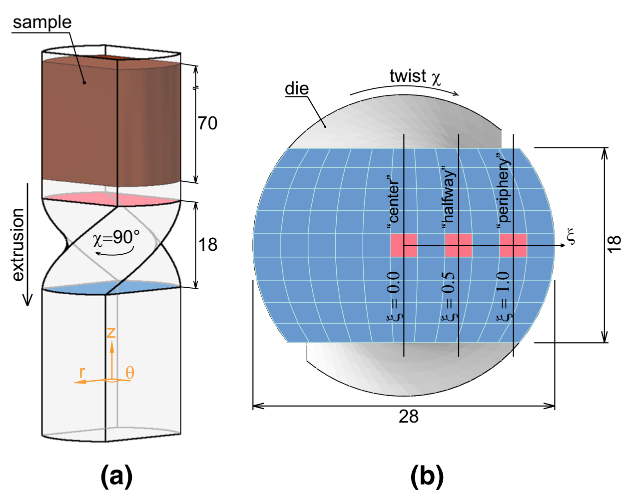

Fig. 1—(*a*) Geometries of the die and the sample used in the experiments and simulations; and (*b*) regions analyzed in the current study in respect to the sample cross section. The vertical lines show approximate locations of surfaces for XRD, optical microscopy, and microhardness measurements (the "halfway" was analyzed only after the first pass). The elements for which the velocity gradient and texture evolution were analyzed are also highlighted. These elements belong to a cross section at the middle of the sample length.

B. *Characterization of Microstructure and Texture*

Grain structures of the as-received and twist-extruded copper were analyzed with optical microscopy. Specimens were cut from the center and periphery regions (Figure 1(b)) parallel to the extrusion axis. The specimens were ground, polished, and then swab-etched for approximately 30 seconds with ASTM etchant #34 (2.5 g $FeCl_3$, 25 ml HCl, 50 ml water).[9]

Textures of the as-received and twist-extruded copper were measured by X-ray diffraction (XRD) in a Bruker D8 Discover diffractometer equipped with a pole-figure goniometer. Four incomplete pole figures—(111), (200), (220), and (311)—were recorded up to a polar angle of 80 deg using CoKα radiation (wavelength 1.79 Å) at 35 kV and 40 mA. The measured intensities were corrected for background and defocussing. Background intensities were calculated as an average of two values recorded at each polar angle on both sides of the peaks. The background intensity was collected 10 times longer than the peak intensity. The peak intensities were further corrected for defocussing based on XRD of a reference sample made of a copper powder embedded in an acryl matrix. Textures were measured in three regions which we shall refer to as "center," "periphery," and "halfway" (shown in Figure 1(b)) after the first TE pass, and in two regions—center and periphery—after multi-pass TE. All XRD measurements were conducted on planes parallel to the longitudinal axis and normal to the radial axis. Orientation distribution functions (ODF) were calculated from the experimental pole figures with the MTEX algorithm.[10] Textures were analyzed through ODF sections and recalculated pole figures. All pole figures in this paper are presented in equal-area projection.

C. *Mechanical Testing*

Microhardness was measured to estimate the effect of multi-pass TE on the mechanical properties of copper and their heterogeneity. Microhardness measurements were conducted with a dwell time of 5 seconds and a load of 500 gf applied to a Vicker's tip. At least 20 indents were made in each specimen for obtaining average microhardness.

For calibrating material model parameters in crystal plasticity finite-element simulations, mechanical behavior of the as-received copper was measured in uniaxial compression at room temperature. Cylindrical specimens for the compression testing had 7 mm in height and 5 mm in diameter. The compression tests were conducted at an initial strain rate of 10^{-3} s^{-1}. Strain was

Table I. Maximum Allowed Concentrations of Impurities in Copper M1 (Russian Nomenclature)

Fe	Ni	S	As	Pb	Zn	Ag	O	Sb	Bi	Sn	Cu
0.005	0.002	0.004	0.002	0.005	0.004	0.003	0.050	0.002	0.001	0.002	99.9

measured with an optical digital image correlation system Aramis. A Teflon film was used to reduce friction between the specimen and the dies.

D. *Modeling and Simulations*

1. *Full-size finite-element simulations of deformation*

A three-dimensional finite-element (FE) model was constructed in commercial FE software ABAQUS for analysis of deformation in the TE process. For the FE model, the actual geometries of the sample and the die channel used in the experiments (Figure 1) were reproduced. The sample was represented by a deformable Lagrangian mesh consisting of 3465 eight-node brick (C3D8) elements with full integration. The die channel was modeled as a rigid surface discretized by four-node shell (R3D4) elements. Simulation of the TE process was performed using Lagrangian analysis in ABAQUS/Standard. Velocity boundary condition in the extrusion direction with a magnitude of 3 mm/s (equal to the actual ram speed) was prescribed to the top nodes of the sample. Finite sliding with tangential behavior (without friction or with friction coefficient, $\mu = 0.05$) was defined for the surface-to-surface contact between the die and the sample. Back pressure of 400 MPa was applied as a surface traction in the counter-extrusion direction to the bottom nodes of the sample. The magnitude of back pressure in FE simulations (400 MPa) was set higher than that in the actual processing (250 MPa) because preliminary FE simulations showed that back pressure defined as a surface traction may underestimate the effect of back pressure: corner gaps were detected in FE simulations with 250 MPa, whereas corner gaps were not observed in the experiments with this magnitude of back pressure.

With the described model of the TE process, two types of constitutive relations were used for modeling of the material behavior. A simple rate-independent model assuming von Mises yield criterion and isotropic perfectly plastic hardening behavior was used in conventional FE method for simulations of the first type

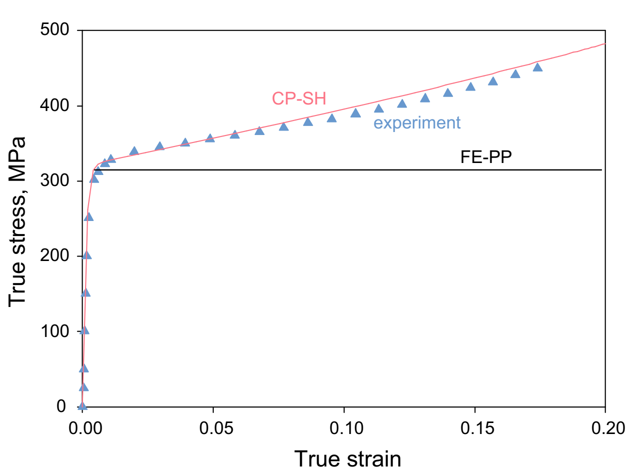

Fig. 2—Stress–strain curves describing the strain-hardening behavior of the material models used in FE and CPFE simulations compared to the experimental data obtained in uniaxial compression.

("FE-PP material") (Figure 2). The second type of simulations was performed in order to take into account plastic anisotropy of the material during deformation. In this type of simulations ("CP-SH material"), the constitutive response of the material was defined by a crystal plasticity theory developed and implemented in FEM by Kalidindi *et al.*[11] In such crystal plasticity FE (CPFE) simulations of fcc metals, only crystallographic slip on $\{111\}\langle 110\rangle$ slip systems is considered to contribute to deformation. The shear rate, $\dot{\gamma}^{\alpha}$ and hardening matrix $h^{\alpha\beta}$ were described by the following equations[12]:

$$\dot{\gamma}^{\alpha} = \dot{\gamma}_0 \left(1 - \frac{\tau^{\alpha}}{s^{\alpha}}\right)^{1/m} \mathrm{sign}(\tau^{\alpha}), \quad [1]$$

$$h^{\alpha\beta} = q^{\alpha\beta} h_0 \left(1 - \frac{s^{\beta}}{s_s^{\beta}}\right)^{a}. \quad [2]$$

Reference values were accepted for initial slip rate ($\dot{\gamma}_0 = 0.001\ \mathrm{s}^{-1}$) and latent hardening ($q^{\alpha\beta} = 1.4$ when $\alpha \neq \beta$),[12] whereas strain-rate sensitivity, m, had to be artificially increased to 0.075 to address convergence problems in full-size CPFE simulations. The other parameters (s_0, h_0, a, s_s) describing single-crystal hardening were obtained by fitting stress–strain curve obtained in simulations of uniaxial compression to the experimental data (Figure 2). The obtained hardening parameters are listed in Table II.

Discrete orientations required for integration points of the deformable mesh were sampled from the ODF obtained from experiments. Each discrete orientation was represented by a set of Euler angles and all orientations had the same statistical weight. Since the as-received copper prior to TE had a non-random texture, the number of orientations belonging to a certain texture component was approximately proportional to the intensity of this component in the ODF. Discrete orientations sampled in this manner were randomly assigned to the integration points.

2. *Polycrystal plasticity simulations of texture evolution*

Analysis of texture evolution during the first TE pass was focused on several elements of a cross section at the middle of the sample length. Three elements were picked from locations which correspond to experimental measurements of texture. These elements (shown in Figure 1(b)) are referred to as "center element" ($\xi = 0$), "halfway element" ($\xi = 0.5$), and "periphery element" ($\xi = 1$), in accord with designation of regions of the experimental texture measurements in the actual sample.

Texture evolution was simulated by subjecting a polycrystalline aggregate to deformation history obtained from full-size FE simulations for the FE-PP and CP-SH materials. In polycrystal plasticity simulations, the material was assigned perfectly-plastic behavior and the same slip resistance as in full-size FE simulations for the CP-SH material. The polycrystalline aggregate consisted of 1200 grains whose orientations were sampled from the ODF of the initial texture in the

Table II. Single-Crystal Hardening Parameters Obtained by Curve Fitting

Initial Slip Resistance, s_0	Parameter, h_0	Parameter, a	Saturation Slip Resistance, s_s
107.5 MPa	20 MPa	3.0	140 MPa

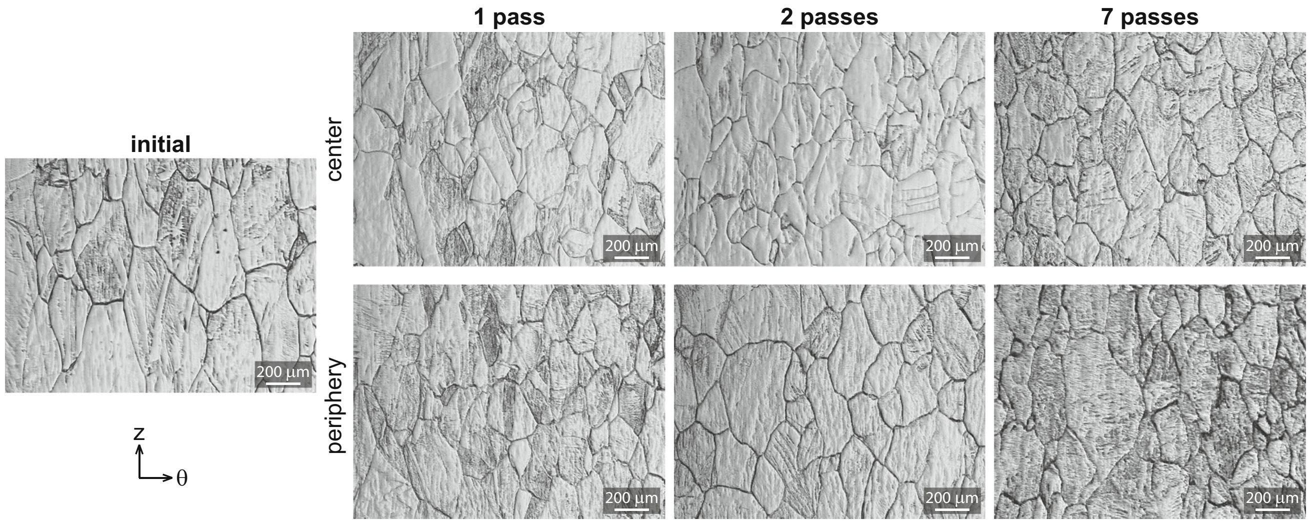

Fig. 3—Optical micrographs of initial and twist-extruded copper in two regions: center ($\xi = 0$) and periphery ($\xi = 1$).

same manner as for full-size CPFE simulations. For modeling texture evolution, two types of polycrystal plasticity simulations were performed. In the first type—Taylor simulations—grains within the polycrystalline aggregate were assumed to experience the same strain as the whole aggregate. For simulations of the second type—polycrystal CPFE simulations—the elements of interest from the full-size FE model were subdivided into 1200 finer elements. The elements of the finer mesh in the polycrystal CPFE model were randomly associated with the same discrete orientations as for the Taylor simulations. As a result, grain–grain interactions were explicitly taken into account in such polycrystal CPFE simulations.

III. RESULTS

A. *Optical Microscopy and Hardness*

To assess the microstructure response to processing by TE, grain structures of as-received and twist-extruded copper were analyzed with optical microscopy (Figure 3). Optical micrographs reveal rather equiaxed grains in all samples. The hot-pressed copper is characterized by coarse-grained structure: grains with diameters in a range of 0.1–0.5 mm are seen in the micrograph. In twist-extruded samples, grains become finer as the number of passes increases; however, large grains are still present in multi-pass samples, and the grain structure even after seven passes is relatively coarse.

Mechanical properties and their heterogeneity were evaluated through microhardness measurements in two regions: center and periphery. The mean values (Table III) indicate that microhardness in the center of the twist-extruded samples slightly increases with the number of passes but remains comparable with that of the as-received sample. Microhardness in the periphery is noticeably higher compared to that of the as-received copper; however, it remains nearly unchanged with increasing pass number. Little or no increase in hardness or other strength characteristics during multi-pass TE was also observed in previous studies.[1,13–16]

Table III. Mean Vickers Microhardness (HV) of the As-Received and Twist-Extruded Copper in the Center and Periphery Regions

	Center	Periphery
Initial	110.26 ± 5.30	
1 pass	108.44 ± 4.08	125.09 ± 5.49
2 passes	113.39 ± 3.32	127.37 ± 4.40
7 passes	115.46 ± 3.32	127.29 ± 3.16

Standard deviation of the measurements was calculated to represent the error.

B. *Texture*

1. *Initial texture and texture gradient after the first pass*

We begin our analysis of textures from inspecting pole figures obtained for copper before and after the first TE pass (Figure 4). Textures were measured at various locations along the major axis of the sample cross section. In the current study, copper in an as-received state was used for processing and thus had a non-random texture prior to TE, which is evident from a (111) pole figure projected along the longitudinal axis.

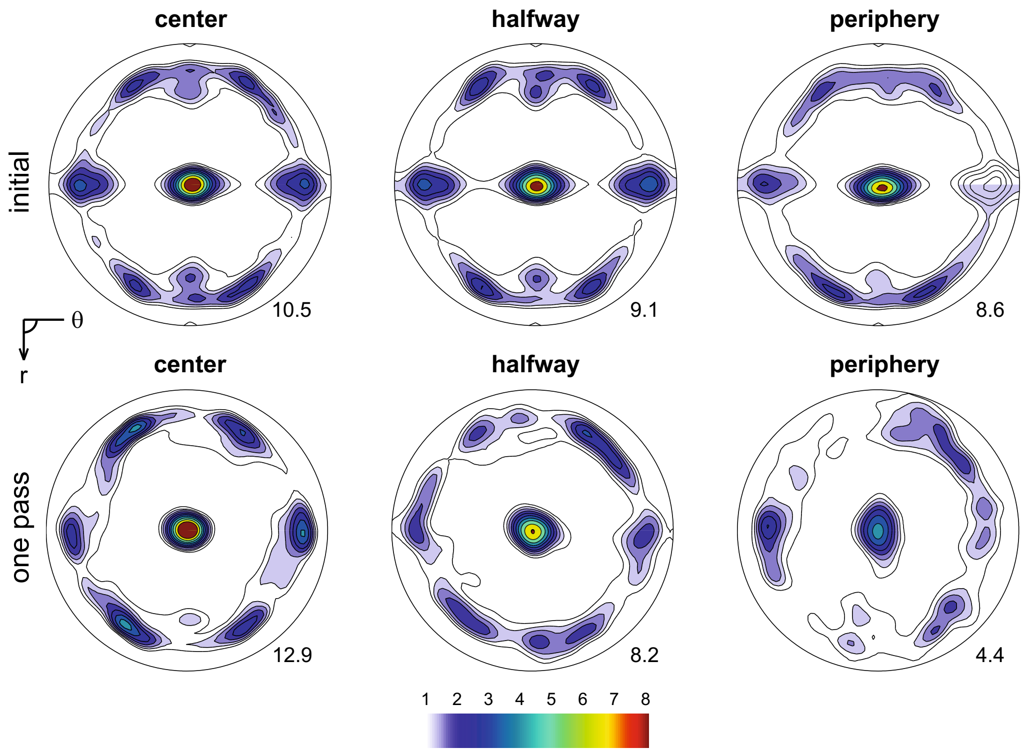

Fig. 4—Recalculated (111) pole figures of textures before and after one pass of twist extrusion obtained from XRD measurements. The pole figures are shown for the center ($\xi = 0$), halfway ($\xi = 0.5$), and periphery ($\xi = 1$) regions. These pole figures are projected along the longitudinal (or extrusion) axis. The numbers indicate maximum pole intensities of the pole figures. Contours: 1.0/1.3/1.6/2.0/2.5/3.2/4.0/5.0/6.4/8.0.

The as-received copper was produced by hot extrusion, an axisymmetric process, for which a combination of $\langle 111 \rangle$ and $\langle 100 \rangle$ fibers can be expected for an fcc metal deforming by slip.[30] The pole figure for the center region shows that, although non-ideal, $\langle 111 \rangle$ fiber is indeed present, which is evident from the intensity peak at the center of the pole figure and a circle of increased intensity towards the rim of the pole figure. At the same time, complete $\langle 100 \rangle$ fiber is not seen: there are only four rather small intensity peaks instead of typical circle of increased intensity. Deviations of the initial texture in the center region of the sample from ideal axial symmetry can be expected to result from thermomechanical treatment of the as-received copper samples before the final operation (conventional hot extrusion).

Pole figures obtained for other regions of the initial sample (halfway and periphery) are qualitatively similar to the pole figure of the center region with some difference in texture strength: texture in the periphery is weaker with a difference in maximum pole intensity of ~2.0.

Pole figures of copper after one TE pass also demonstrate a non-uniform texture (Figure 4). The $\langle 111 \rangle$ fiber persists in all regions but the intensity of the peak decreases in the radial direction from the center to the periphery with texture in the center being sharper than the initial texture. The initial and first-pass textures in different locations differ not only in the $\langle 111 \rangle$ peak intensity but also in the distribution of off-axis intensities. While there are three equally spaced off-axis concentrations of higher intensity in the pole figure of the initial texture, the pole figure for the first-pass-center specimen has six well-defined off-axis peaks. Similar peaks are found in the texture at $\xi = 0.5$ but, in this case, they are less clearly defined and spread more uniformly around the longitudinal axis. The specimen of the periphery region reveals again three but weaker off-axis intensity concentrations.

For a better understanding of texture after the first TE pass, sections of orientation distribution functions (ODFs) were examined. Since TE is a shear-based process, it is beneficial to analyze ODF sections in respect to ideal orientations established for simple shear.[17,18] Ideal orientations in simple shear and their development were exhaustively treated in literature dedicated to torsion[19–21] or equal channel angular pressing (ECAP).[22–24] We shall only remind that ideal orientations depend on the crystal structure and, for fcc crystal structures, they are A, $\bar{A}$, A_1^*, and A_2^* components forming the partial A fiber, and A, $\bar{A}$, B, $\bar{B}$, and C components forming the partial B fiber.[25] For making the ODFs of first-pass textures in copper comparable with ideal shear orientations, the ODFs are referenced to simple shear frame, in which shear plane normal points up whereas shear directions lie in horizontal plane.

Figure 5 depicts ODF sections of the initial and twist-extruded copper with superimposed ideal orientations of simple shear. The ODF sections of the initial texture demonstrate that, even before TE, texture of the as-received copper had maxima coinciding with the A, $\bar{A}$, A_1^*, and A_2^* components. At the same time, B and $\bar{B}$ components are not present in the initial texture of

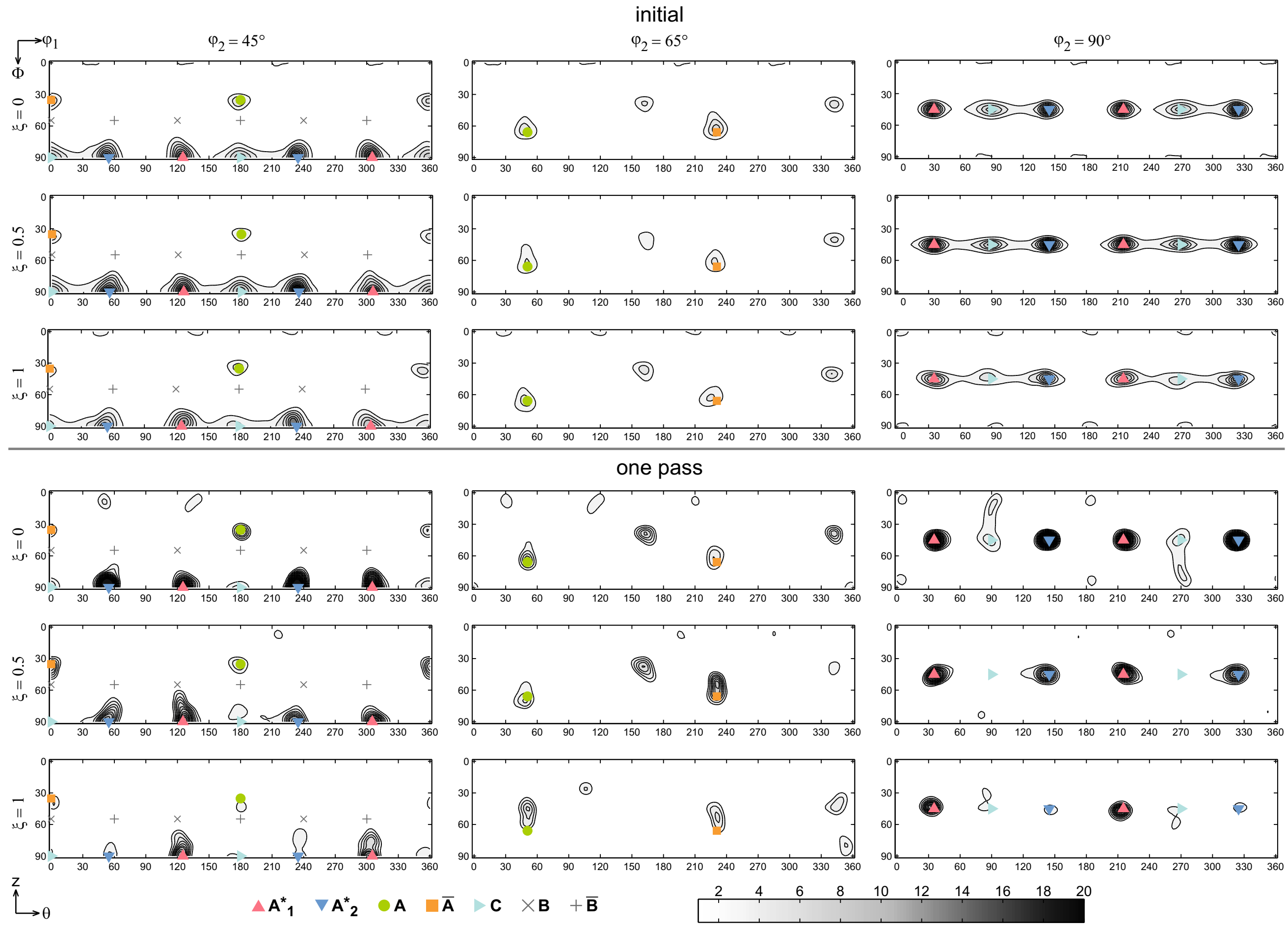

Fig. 5—Sections of orientation distribution functions estimated from XRD measurements for copper before and after one pass of twist extrusion. The sections are shown for the center ($\xi = 0$), halfway ($\xi = 0.5$), and periphery ($\xi = 1$) regions. Contours: 3.0/4.2/5.5/6.6/7.8/9.0/10.0/11.5/12.7/13.9/15.0/16.3/17.5/18.7/20.0.

copper. The ODF sections of the initial texture also indicate some texture heterogeneity present prior to TE: the intensity of ODF of the edge region ($\xi = 1$) is lower than those of the center ($\xi = 0$) and halfway regions ($\xi = 0.5$).

ODF sections of the first-pass texture in all regions are qualitatively alike and resemble those of the initial texture. The major difference between the initial and first-pass textures lies in the intensities. As in the case of the initial texture, the ODF sections in the center ($\xi = 0$) after one pass reveal high intensities at both A_1^* and A_2^* positions with the A_2^* component being slightly stronger. Towards the periphery of the sample cross section, however, the A_2^* component diminishes, whereas the A_1^* component also weakens to some extent but becomes a component of the highest intensity in regions towards the periphery of the sample cross section ($\xi = 0.5$ and 1). We finally note that although the initial and first-pass textures are found to have intensity peaks at ideal shear orientations, the A and B fibers are not observed in the first-pass textures.

2. *Texture evolution in multi-pass twist extrusion*

It is also essential to understand the effects of performing multiple passes on texture evolution during TE. This is because multi-pass TE is frequently required for improving mechanical properties and their distribution throughout the sample. For finding effects of multi-pass TE on texture of copper, textures after two and seven passes were measured. The analysis of multi-pass textures was focused on the center and periphery regions because the results on the first-pass textures suggested that the texture at $\xi = 0.5$ can be characterized as a transition texture between those at $\xi = 0$ and 1.

Multi-pass textures along with the initial and one-pass textures are shown in (111) pole figures projected along the radial axis (Figure 6), which makes the shear plane normal vertical and shear directions horizontal. The pole figures show that texture evolution differs in the center and the periphery. In the center, features of the $\langle 111 \rangle$ fiber inherited from the initial texture retain even after seven passes. The maximum pole intensity increased after the first pass decreases with further processing. Texture weakens in the periphery as well: maximum pole intensity drops after the first pass to 4.4 (multiples of uniform distribution) m.u.d., decreases by 50 pct after the second pass to 2.8 m.u.d., and changes only slightly from that after seven passes—2.6 m.u.d. In the periphery, however, not only does pole intensity

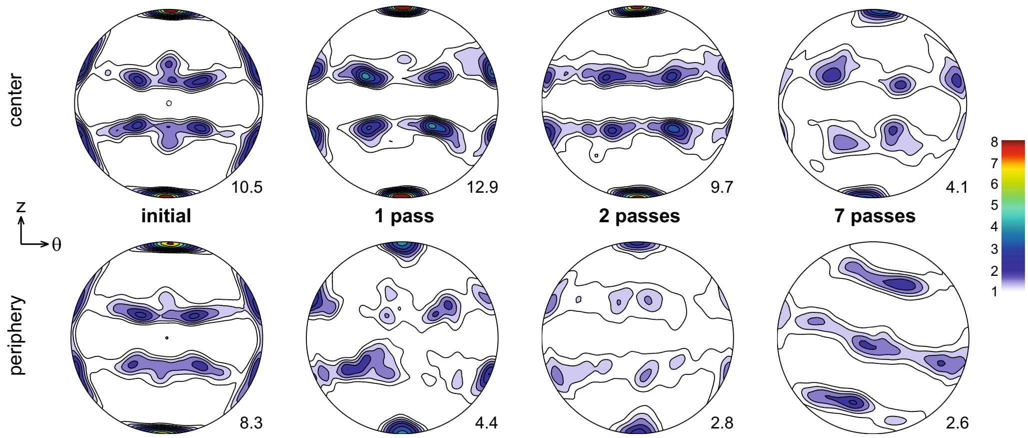

Fig. 6—Pole figures of as-received and twist-extruded copper after one, two, and seven passes of twist extrusion. For processed samples, textures are shown for both center ($\xi = 0$) and periphery ($\xi = 1$) regions. These pole figures are projected along the radial axis, which makes the shear plane normal vertical and shear directions horizontal during twist extrusion. Contours: 1.0/1.3/1.6/2.0/2.5/3.2/4.0/5.0/6.4/8.0.

change, but also the character of texture after different numbers of passes. Like the first-pass textures, the texture after two passes has texture components related to simple shear; however, in this case they are weaker, less defined and more spread around the longitudinal axis compared to the first-pass textures. The texture in the periphery after seven passes is more noticeably different from the initial, one-pass, and two-pass textures. Instead of the $\langle 111 \rangle$ fiber, it has a tilted $\langle 110 \rangle$ fiber, in which $\langle 110 \rangle$ crystal axes are inclined to ~15 deg in respect to the longitudinal axis of the specimen (*i.e.,* extrusion axis).

For analysis of weakening of texture in multi-pass TE in a more quantitative manner, texture index was calculated. Texture index, J, of an ODF, $f(g)$, is a scalar quantity concisely describing texture strength, which can be obtained using the following expression.[26]

$$J = \oint [f(g)]^2 dg. \qquad [3]$$

Results of calculations of the texture index (performed in MTEX toolbox) for the initial and twist-extruded copper are presented in Table IV for the two regions under study. Texture index for the center region raises after the first pass and then continuously decreases with the number of passes, which is consistent with the trend of maximum pole intensities in (111) pole figures analyzed above. In the periphery, however, texture index drops during the first two passes but is found increased after seven passes. Another tendency to be noted is a decrease in the difference between values of the texture index in the two regions. Indeed, after the first pass, texture index in the center is more than two times that in the periphery, which signifies a marked spatial variation of the texture strength in the sample. After seven passes, in contrast, the values of the texture index are nearly identical, which makes the seven-pass sample more uniform in terms of the texture strength variations.

Table IV. Texture Index of the As-Received and Twist-Extruded Copper in the Center and Periphery Regions

	Center	Periphery
initial	3.9	3.1
1 pass	4.9	2.0
2 passes	3.2	1.3
7 passes	1.7	1.6

C. *Modeling and Simulations*

1. *Deformation history*

Analysis of deformation history is essential for understanding of texture evolution. Although deformation history during TE was already addressed in the literature in terms of equivalent plastic strain[27] or strain rate tensor,[3] understanding of texture evolution requires knowledge of velocity gradient, which takes into account both stretches and rotations.[25] Therefore, the evolution of the velocity gradient during TE for relevant combinations of the material and processing factors was analyzed in the present work. Velocity gradient $\mathbf{L}'$ was derived from deformation gradient $\mathbf{F}$ as proposed by Li *et al.*[28]:

$$L'_\tau = (F_\tau F_t - I)/\Delta t, \qquad [4]$$

where $\mathbf{I}$ is the identity tensor, $\Delta t = \tau - t$ is the time increment with τ and t denoting times of the end and the beginning of the time increment, respectively. Deformation tensors reveal the deformation character in TE better if they are expressed in a cylindrical coordinate frame.[3] The velocity gradient in cylindrical coordinates $r\theta z$ (shown in Figure 1(a)) was obtained through a transformation $[L] = [Q]\ [L']\ [Q]^{\mathrm{T}}$ with $[Q]$ being a transformation matrix from Cartesian to cylindrical coordinates. The evolution of the resulting tensor $\mathbf{L}$ in the elements of interest is shown for the FE-PP material deforming with no friction (Figure 7(a)) as well as for the CP-SH material deforming with (Figure 7(c)) or without (Figure 7(b)) friction.

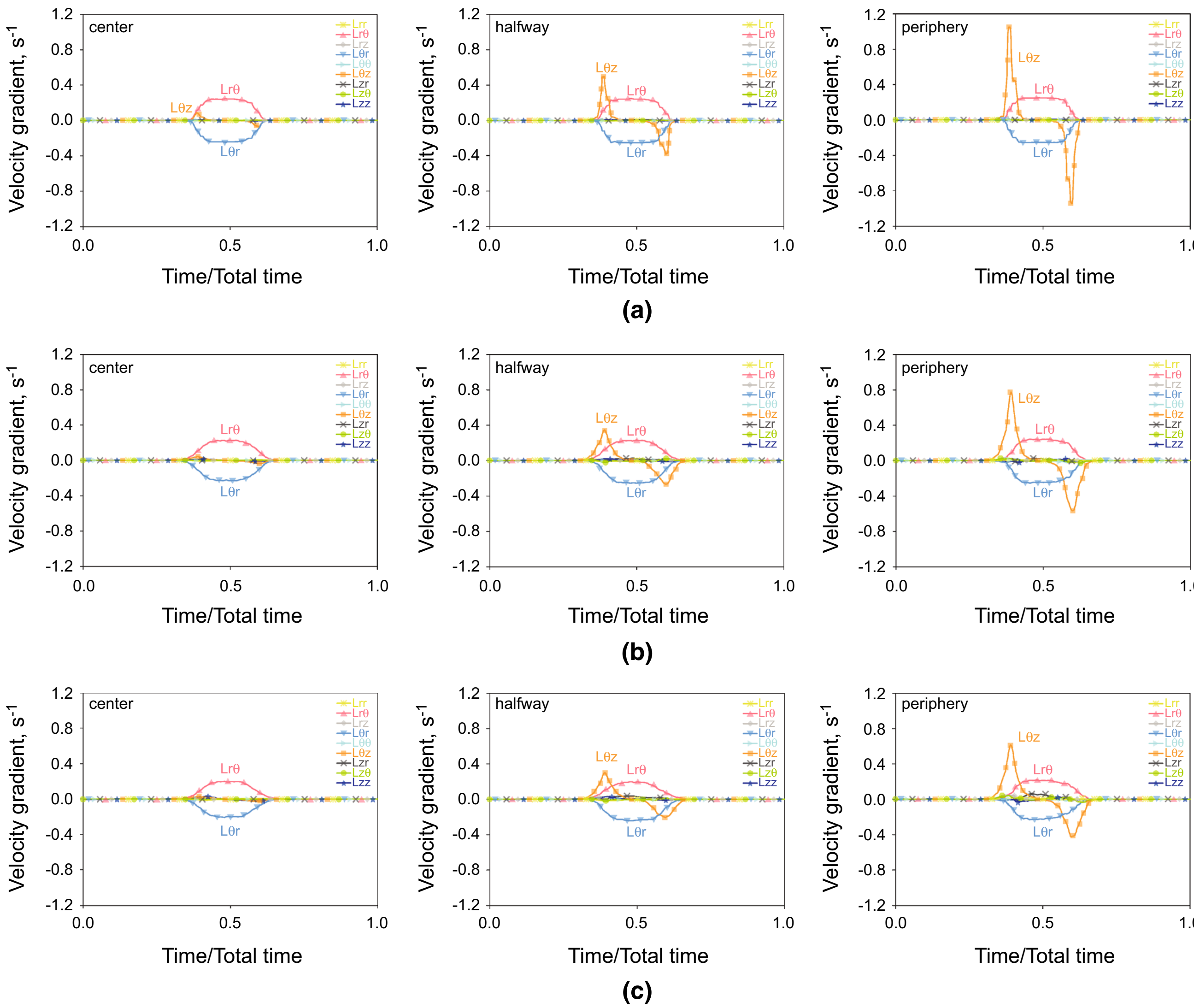

Fig. 7—Evolution of the velocity gradient for the center ($\xi = 0$), halfway ($\xi = 0.5$), and periphery ($\xi = 1$) elements. Curves are obtained for (*a*) FE-PP material with no friction, (*b*) CP-SH material with no friction, and (*c*) CP-SH material with friction.

For all studied cases and regions, the velocity gradient departs from zero only when the element goes through the twist channel. In the twist channel, the components of the most significant magnitudes are off-diagonal components, $L_{r\theta}$, $L_{\theta r}$, and $L_{\theta z}$. Their evolution and relative magnitudes depend on the location of the element and the strain-hardening behavior of the material.

In the center element ($\xi = 0$), the components $L_{r\theta}$ and $L_{\theta r}$ have the highest magnitude for both FE-PP and CP-SH materials. These components are characterized by nearly identical magnitudes but opposite signs, *i.e.*, $L_{r\theta} \approx -L_{\theta r}$. The fact that $L_{r\theta}\ L_{\theta r} = 0$, while the other components are negligible, indicates rigid body rotation of the element[29]—in this case—around the longitudinal axis. Although rigid body rotation is dominant for the center element, some small peaks of the component $L_{\theta z}$ can also be noticed, especially in the case of deformation history obtained for the FE-PP material (Figure 7(a)). For the CP-SH material (Figures 7(b) and (c)), the components $L_{r\theta}$ and $L_{\theta r}$ increased more gradually as the element was approaching the twist channel.

For the periphery element ($\xi = 1$), the evolution of the components $L_{r\theta}$ and $L_{\theta r}$ is similar to that obtained for the center element and indicates rigid body rotation around the extrusion axis. In contrast to the center region, however, the component of the highest magnitude in the periphery is the shear component $L_{\theta z}$. For the FE-PP material (Figure 7(a)), the component $L_{\theta z}$ has a sharp positive peak (indicating positive shear) at the first intersection plane and a nearly identical peak of the opposite sign (indicating negative shear) at the second intersection plane. The evolution of the component $L_{\theta z}$ signifies that deformation in this case is close to ideal deformation described by the simple shear model.[3] According to the simple shear model, deformation in TE consists of two simple shear deformations of the same magnitude but opposite sense acting on two narrow intersection planes. The simple shear model holds strictly only for PP materials and without friction between the sample and the die.[3] The same can be concluded from the evolution of the velocity gradient obtained in the present study: the CP-SH material deforms in much broader plastic deformation zones (PDZs) (Figure 7(a)) compared to theoretically assumed narrow PDZs along the intersection planes. Furthermore, deformation of the CP-SH material is different in the two PDZs as can be seen from two peaks of the component $L_{\theta z}$ that differ in both maximum and shape. Evolution of the velocity gradient obtained for TE of the CP-SH material in the presence of friction between the sample and the die is shown in Figure 7(c). It is seen that friction also causes broadening of the PDZs. Furthermore, friction results in departure of the other components of the velocity gradient from zero, especially in the periphery region. It means that, although simple shear is still prevailing deformation, friction between the sample and the die leads to a more complex deformation mode.

The evolution of the velocity gradient obtained for the halfway element ($\xi = 0.5$) is overall similar to that of the periphery element. The main difference from the periphery is that the magnitude of shear deformation is smaller in the halfway element as can be seen from the evolution of the component $L_{\theta z}$. Furthermore, the friction effects are less significant in the case of the halfway element (Figure 7(c)).

2. *Predictions of the first-pass textures*

Having the history of the velocity gradient in hand allows for performing polycrystal plasticity simulations of texture evolution during TE. Texture evolution was simulated by subjecting a polycrystalline aggregate consisting of 1200 "grains" to FE deformation histories obtained for the FE-PP and CP-SH materials with and without friction.

As a first approach, the grains in the aggregate were assumed to undergo the same deformation as the whole aggregate (Taylor simulations). Figure 8 shows textures in the periphery region predicted with the Taylor simulations through (111) pole figures and $\varphi_2 = 45°$ ODF sections. Texture predictions are presented for three stages: at the beginning (before PDZs, initial texture), middle (after the first PDZ), and end (after PDZs, final texture) of the process. As pointed out in the previous section, during TE, the sample undergoes rigid body rotation around the extrusion axis to an angle equal to the twist angle, which is 90 deg clockwise for the present die. To compensate for the rigid body clockwise rotation of the sample around the extrusion axis, ODFs obtained from simulations for the middle and end of the process were rotated counter-clockwise to 45 and 90 deg, respectively, around the extrusion axis. Such compensation makes textures for different stages of the process readily comparable.

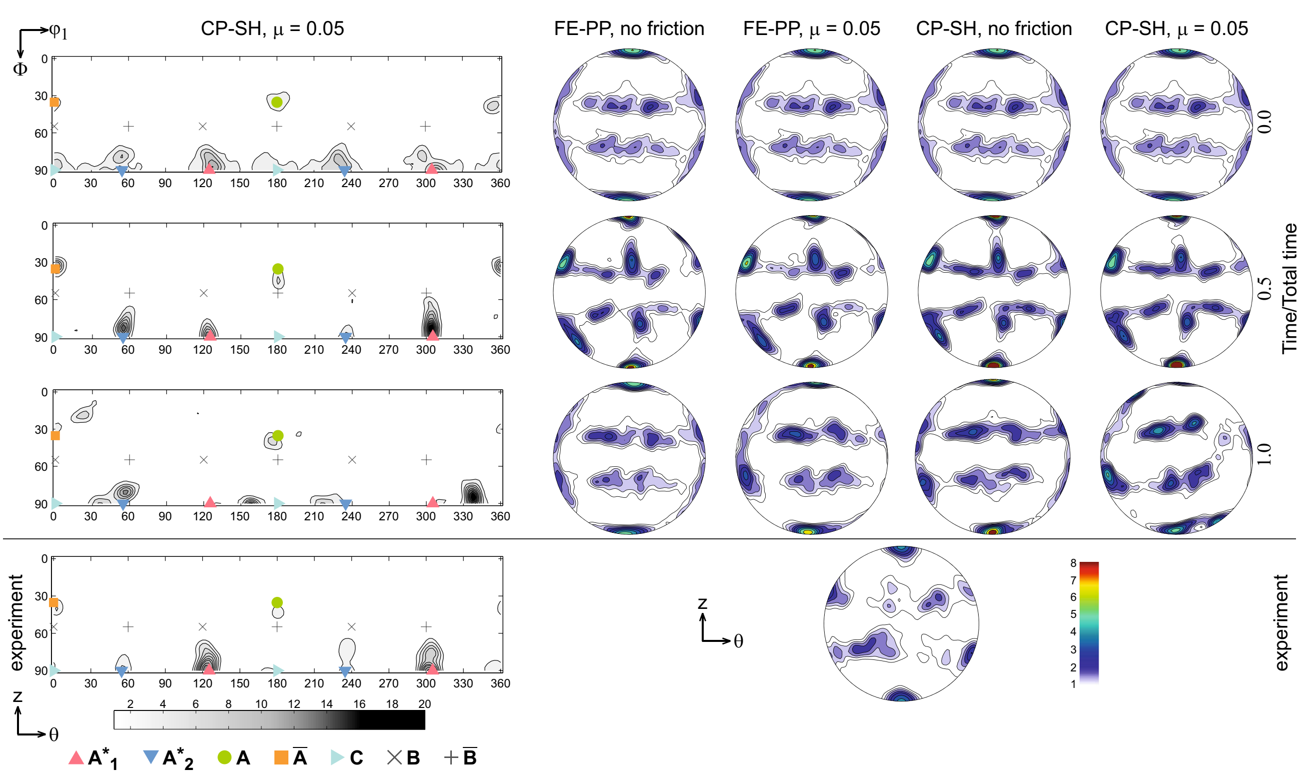

Fig. 8—Textures obtained in Taylor simulations for the periphery region with different FE deformation histories. The figure depicts ODF sections of $\varphi_2 = 45°$ for deformation history of CP-SH material with friction and (111) pole figures for deformation histories of FE-PP and CP-SH materials with or without friction. The pole figures are projected along the radial axis. The ODF section and pole figure of experimental first-pass texture are also shown. Pole figure contours: 1.0/1.3/1.6/2.0/2.5/3.2/4.0/5.0/6.4/8.0. ODF contours: 3.0/5.5/7.8/10.0/12.7/15.0/17.5/20.0/22.0/24.7/27.0/29.5.

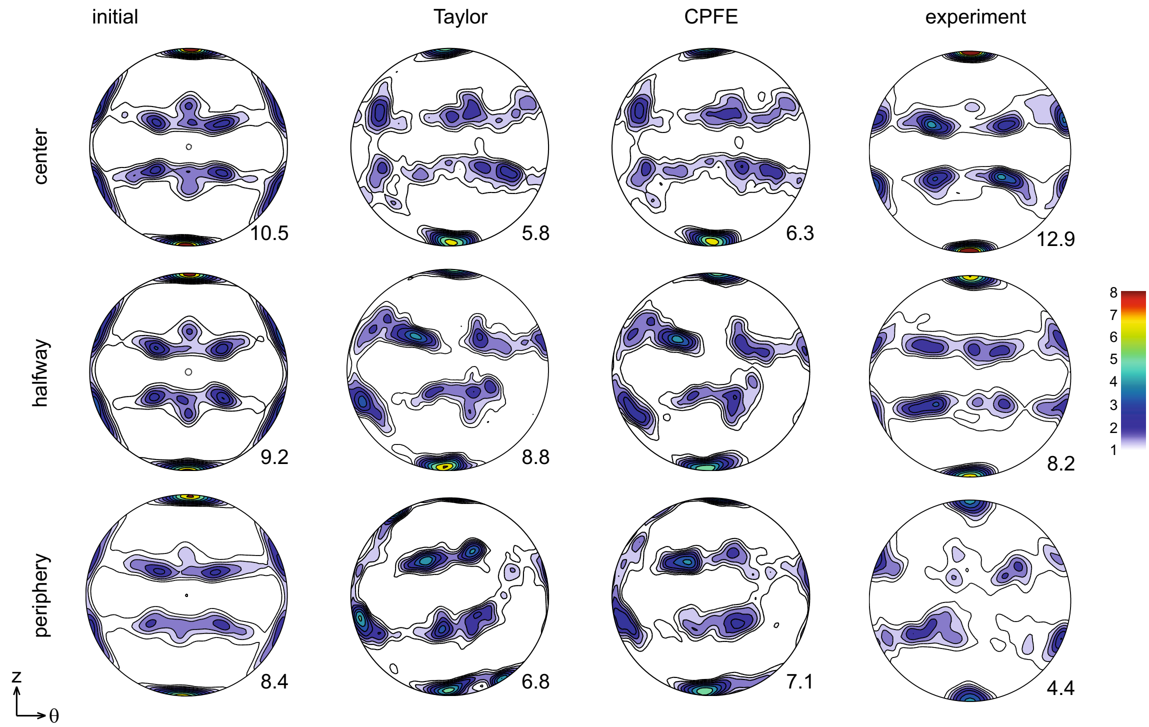

Fig. 9—Comparison between Taylor predictions, CPFE predictions and measurements of the final first-pass textures in the center ($\xi = 0$), halfway ($\xi = 0.5$), and periphery ($\xi = 1$) regions. Textures are represented through (111) pole figures. The numbers indicate maximum pole intensities of the pole figures. Contours: 1.0/1.3/1.6/2.0/2.5/3.2/4.0/5.0/6.4/8.0.

The results of these simulations shed some light on important details of texture evolution in TE as well as on performance of polycrystal plasticity simulations. First of all, in all studied cases, texture components related to simple shear form during deformation in the first PDZ. Comparison of predictions obtained with different FE deformation histories demonstrates that textures after the first PDZs are overall alike with only minor differences. Under the frictionless condition, texture after the first PDZ is almost identical in both FE-PP and CP-SH cases. The presence of friction leads to a slightly different texture development in the first PDZ as well as to more noticeable differences between textures obtained for FE-PP and CP-SH materials.

Simulated textures after the second PDZ indicate that, in the second PDZ, texture is partially recovered to the initial state. The texture reversal is nearly complete in the FE-PP case, especially under the frictionless condition. As strain reversal is imperfect in the case of the CP-SH material, especially in the presence of friction, Taylor simulations predict final texture different from the initial one. At the same time, it is evident that, even with these deformation histories with imperfect strain reversal, Taylor simulations do not capture the measured texture. The disagreement between the predictions and measurements is especially clear in the $\varphi_2 = 45°$ ODF sections. While the ODF estimated from the experimental measurements have a maximum around the A_1^* ideal orientation with much lower intensity at the A_2^* position, the simulations for the CP-SH material deforming with friction predict the maximum intensity at the A_2^* position.

In an attempt to improve agreement between the predictions and measurement, another set of polycrystal plasticity simulations taking grain–grain interactions into account was conducted. For these CPFE simulations, the elements of interest from full-size FE simulations were subdivided into a finer mesh consisting of 1200 elements. These elements were directly associated with "grains" and thereby constituted a polycrystalline aggregate. The aggregate was subject to the same FE deformation histories as in Taylor simulations.

The first-pass textures predicted by such CPFE simulations are shown in Figure 9 for the center, halfway, and periphery regions and compared with Taylor predictions as well as experimentally measured textures. The results demonstrate that CPFE predictions are overall similar to those of Taylor simulations. The main difference lies in that some components in CPFE-predicted textures were less sharp and more diffuse. Most importantly, however, CPFE predictions also did not capture experimentally observed texture although grain–grain interactions were taken into account and FE deformation history with imperfect reversal of strains was used.

IV. DISCUSSION

A. *Texture Elimination During Twist Extrusion*

Measurements of texture evolution conducted in the current study demonstrate that multi-pass TE is effective for mitigating preferred orientations in pre-textured copper. The observation of texture-weakening as a result of TE is consistent with the earlier texture measurements in hot-rolled Ti after TE.[7] The main reason for a decrease in texture strength during the process can be that simple shear is a prevailing deformation in TE. Simple shear is known to result in relatively weak textures because there are no ultimate stable orientations; instead, there are orientation *ranges* where grain rotation slows down.[30] Furthermore, it was demonstrated in the current and previous[3] FE studies that reversal of shear strains takes place during TE, which can further contribute to elimination of preferred orientations. Indeed, very weak textures were reported for torsion-reverse torsion experiments[31,32] and ECAP route C.[28]

Texture in multi-pass TE became weak not only in the periphery region, where shear strains and their reversal are largest, but also in the central region. Decrease in texture strength in the center can be caused by small shear strains found with the FE simulations (Figure 7). With these findings, we conclude that processing regimes utilizing multi-pass TE can be adjusted for producing metallic samples with uniformly weak textures. This ability of the process can be particularly useful in cases when texture-induced anisotropy of properties is unfavorable in further processing or actual service of metallic materials.

B. *Effects of the Initial Texture*

In the current study, copper was processed by TE in an as-received state and had a non-random initial texture. Results of the present study allow for deducing some effects of the initial texture in as-received copper. First, the initial texture was non-uniform prior to TE as a result of hot extrusion: the periphery texture was weaker than that near the axis of the sample (Table IV). The spatial heterogeneity of the initial texture was therefore likely to contribute to the texture gradient observed after 1 to 2 TE passes. At the same time, strain gradients imposed by TE are thought to have a more pronounced effect than the initial texture heterogeneity as the difference in texture index between the center and periphery region in the first-pass texture is larger compared to that in the initial texture.

Second, the initial texture present in copper in the current study may have affected formation of texture fibers characteristic of simple shear deformation. Texture developing in simple shear deformation is known to include partial *A* and *B* fibers.[25] At the same time, polycrystal plasticity simulations in the current study showed that these fibers do not form during deformation in the first PDZ. It suggests that the initial texture of as-received copper can prevent the formation of the *A* and *B* fibers during simple shear deformation in TE. This effect of the initial texture is evident from predictions of polycrystal plasticity simulations with different initial textures: actual from experimental measurements and random. From the predicted textures in such simulations (Figure 10), it is evident that, while the *A* and *B* partial fibers fully develop when the initial texture was random, the actual initial texture prevented their

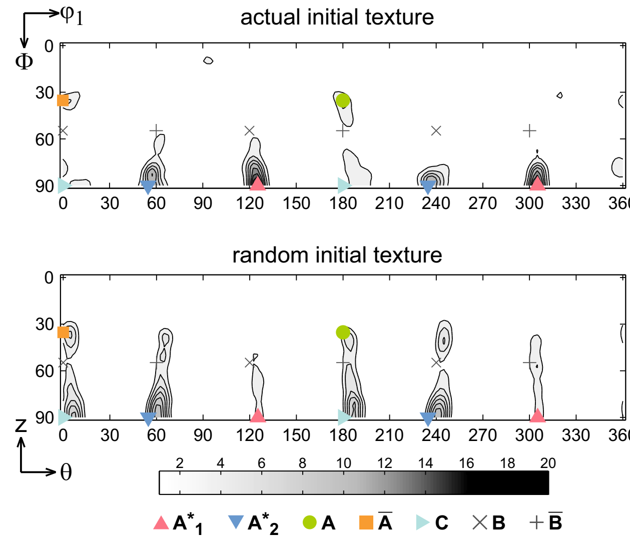

Fig. 10—Effect of the initial texture on formation of the ideal simple shear fibers illustrated in $\varphi_2 = 45°$ ODF sections. The ODF sections are obtained in CPFE simulations after the first PDZ. CPFE simulations were run with the deformation history obtained for the FE-PP material under frictionless condition. Contours: 3.0/4.2/5.5/6.6/7.8/9.0/10.0/11.5/12.7/13.9/15.0/16.3/17.5/18.7/20.0.

formation during simple shear deformation in the first PDZ. This finding accounts for experimental observations that the *A* and *B* fibers were absent in the first-pass textures, whereas ideal shear components were present (Figure 5).

Another possible effect of the initial texture is moderate grain refinement (Figure 3) compared to previous reports on microstructures in twist-extruded metals.[1,33,34] Inspection of ODF sections showed that the initial texture of copper produced by hot pressing already had some orientations stable in simple shear deformation in TE (Figure 5). The presence of such stable orientations during deformation may decrease tendency of grains to subdivide and therefore can account for more moderate increase in hardness in the current study compared to previous TE experiments (*e.g.,*[15]) with metals annealed prior to TE processing.

C. *Strain Reversal Texture in Twist Extrusion*

Current polycrystal plasticity simulations of texture evolution in the first pass of TE predicted nearly complete recovery of texture to the initial state upon reversal of shear strains in the case of FE deformation histories obtained for the frictionless process. However, such texture recovery was not observed experimentally (Figures 6 and 9). It is interesting that texture reversal was predicted even by CPFE simulations (Figure 9), which directly take into account grain–grain interactions. Generally, such CPFE simulations were expected to perform better[28,35] than Taylor simulations. It appears that modeling of texture evolution in TE runs into the problem of strain reversal texture, which is well known in modeling of texture in ECAP route C. For ECAP route C, several phenomena were pointed out to be responsible for disagreement between the experiment and predictions[25]: imperfect reversal of shear strains; grain refinement; inhomogeneous deformation through the sample thickness, and others.

It was reasonable to anticipate that imperfect reversal of shear strains contributes to the occurrence of strain reversal texture in TE. Earlier experimental investigations of metal flow in TE with a marker-insert technique demonstrated that deformation in TE can significantly deviate from the ideal deformation (with perfect strain reversal) described by the simple shear model.[36,37] Recently, it was shown with FE simulations that experimentally found deviations from the ideal deformation originate, for the most part, from friction between the sample and the die.[3] Factors that lead to non-ideal deformation (*i.e.,* friction and high strain-hardening rates of the material) also result in that deformation in each PDZ is different and thus reversal of shear strains is imperfect. With the knowledge of the importance of non-ideal deformation in TE, FE simulations taking friction and strain-hardening behavior of the material were conducted in the current study. Both Taylor and CPFE simulations performed with FE deformation histories taking friction into account predicted final textures different from the initial texture. Nevertheless, even with such more accurate FE deformation histories, the agreement between texture predictions and experimental measurement were not satisfactory (Figures 8 and 9).

Discrepancies between predicted and measured textures suggest that imperfect reversal of shear strains in TE is a contributing but not the only factor of development of strain reversal texture in TE. Furthermore, strain reversal texture was also observed in torsion–reverse torsion experiments[31,38] where it is much more feasible to assure perfect reversal of shear strains compared to TE or ECAP. Summarizing reports on final textures in torsion–reverse torsion experiments, Wu *et al*.[32] suggested that the final texture and its strength depend on the amplitude of shear deformation: the larger forward shearing (and thus the amplitude), the stronger the strain reversal texture retained from the first deformation. Zhu and Lowe[39] also stated that it may be easier to restore the initial texture. Interestingly, such a dependence of the strain reversal texture on the shear amplitude appears to take place in TE too. Indeed, while the periphery region of the sample was clearly characterized by shear texture, the textures in the other regions (halfway and center) were more similar to the initial texture (Figure 9).

Grain subdivision was proposed to be the origin of strain reversal texture in the case torsion–reverse torsion deformation.[31] The key role of grain refinement in strain reversal texture explains the dependence of strain reversal texture on the magnitude of forward shearing: the larger the magnitude, the more intensive grain refinement and, thus, the stronger strain reversal texture. The virtue of incorporating grain refinement in polycrystal plasticity models was demonstrated in the case of ECAP route C. Indeed, the use of a recent grain refinement model[40] for ECAP route C improved agreement between measured and predicted textures.[41]

In this light, the use of polycrystal plasticity models that incorporate grain refinement (*e.g.,* that of Toth *et al*.[40]) combined with FE deformation histories can be expected to yield the best predictions of texture in TE. Therefore, such simulations are recommended for further research on modeling of texture evolution in TE. Finally, the material asymmetry under reverse loading was not considered in the current study, whereas it may also contribute to the texture evolution so that taking into account slip direction (*e.g.,*[42]) and back stresses (*e.g.,*[43]) can be also beneficial.

V. SUMMARY

A combination of characterization and modeling of texture evolution in twist extrusion (TE) was carried out for the first time. The results of the study are summarized below.

1. Texture development in copper during TE is non-uniform. The first TE pass led to a marked texture gradient in the radial direction, which resulted from texture heterogeneities in the initial texture of as-received copper and non-uniform deformation imposed by TE. After multi-pass TE, variations of texture strength diminished and samples with uniformly weak texture were obtained.
2. Polycrystal plasticity simulations of texture evolution during the first TE pass predicted return of the initial texture upon strain reversal in deformation histories obtained for frictionless condition. Recovery of the initial texture was not observed experimentally. Instead, texture related to simple shear was found. Taking friction into account in finite-element simulations led to prediction of strain reversal texture, which however was not consistent with experimental measurements.
3. Grain refinement was proposed to be responsible for the occurrence of strain reversal texture in TE. Therefore, polycrystal plasticity models incorporating grain refinement combined with finite-element simulations are recommended for further research on modeling of texture evolution in TE. Consideration of the material asymmetry (slip directionality and back stress) is also expected to improve texture predictions under strain reversal in TE.

In a concluding remark, we note that twist extrusion provides extra space for research of evolution of texture and microstructure under loading with severe strain path changes and large plastic strains.

ACKNOWLEDGMENTS

The authors would like to thank Dr. L.S. Toth for insightful comments on the manuscript. Dr. B.-C. Suh and Dr. Y. Jeong are also gratefully acknowledged for assistance with XRD measurements. The current research was supported by the National Research Foundation of

Korea (NRF) grant funded by the Korea government (MSIP) (No. 2014R1A2A1A10051322).

REFERENCES

1. Y. Beygelzimer, D. Orlov, A. Korshunov, S. Synkov, V. Varyukhin, I. Vedernikova, A. Reshetov, A. Synkov, L. Polyakov, and I. Korotchenkova: *Solid State Phenom*., 2006, vol. 114, pp. 69–78.
2. Y. Beygelzimer, D. Orlov, and V. Varyukhin: in *Ultrafine Grained Materials II*, Y.T. Zhu, T.G. Langdon, R.S. Mishra, S.L. Semiatin, M.J. Saran, and T.C. Lowe, eds., The Minerals, Metals & Materials Society, Warrendale, PA, 2002, pp. 297–304.
3. M.I. Latypov, M.-G. Lee, Y. Beygelzimer, and H.S. Kim: *Met. Mater. Int*., 2015, vol. 21, pp. 569–79.
4. S.A.A. Akbari Mousavi and S.R. Bahadori: *Mater. Sci. Eng., A*, 2011, vol. 528, pp. 1242–46.
5. N.M. Shkatulyak: *Int. J. Adv. Mater. Sci. Eng*., 2014, vol. 3, pp. 15–25.
6. V.V. Usov, N.M. Shkatulyak, P.A. Bryukhanov, and Y. Beygelzimer: *High Pressure Phys. Tech*., 2011, vol. 21, pp. 102–109.
7. V.V. Usov, N.M. Shkatulyak, P.A. Bryukhanov, and Y. Beygelzimer: *High Pressure Phys. Tech*., 2011, vol. 21, pp. 103–108.
8. S.R. Bahadori, K. Dehghani, and S.A.A. Akbari Mousavi: *Mater. Lett*. 2015, vol. 152, pp. 48–52.
9. ASTM Standard E407, 2007e1, *Standard Practice for Microetching Metals and Alloys,* ASTM International, West Conshohocken, PA, 2007.
10. R. Hielscher and H. Schaeben: *J. Appl. Crystallogr*., 2008, vol. 41, pp. 1024–37.
11. S.R. Kalidindi, C.A. Bronkhorst, and L. Anand: *J. Mech. Phys. Solids*, 1992, vol. 40, pp. 537–69.
12. S.R. Kalidindi: PhD Thesis, MIT, Cambridge, 1993.
13. S.V. Dobatkin, G.A. Salishev, A.A. Kuznecov, A. Reshetov, S. Synkov, and T.N. Konkova: *Phys. Tech. High Pressure*, 2006, vol. 16, pp. 23–36.
14. M.I. Latypov, E.Y. Yoon, D.J. Lee, R. Kulagin, Y. Beygelzimer, M.S. Salehi, and H.S. Kim: *Metall. Mater. Trans. A*, 2014, vol. 45A, pp. 2232–41.
15. D. Orlov, Y. Beygelzimer, S. Synkov, V. Varyukhin, N. Tsuji, and Z. Horita: *Mater. Sci. Eng., A*, 2009, vol. 519, pp. 105–11.
16. A. Reshetov, A. Korshunov, A. Smolyakov, Y. Beygelzimer, V. Varyukhin, I. Kaganova, and A. Morozov: *Mater. Sci. Forum*, 2011, vols. 667–669, pp. 851–56.
17. G.R. Canova, U.F. Kocks, and J.J. Jonas: *Acta Metall*., 1984, vol. 32, pp. 211–26.
18. L.S. Toth, P. Gilormini, and J.J. Jonas: *Acta Metall*., 1988, vol. 36, pp. 3077–91.
19. B. Beausir, L.S. Tóth, and K.W. Neale: *Acta Mater*., 2007, vol. 55, pp. 2695–2705.
20. F. Montheillet, P. Gilormini, and J.J. Jonas: *Acta Metall*., 1985, vol. 33, pp. 705–17.
21. L.S. Tóth, K.W. Neale, and J.J. Jonas: *Acta Metall*., 1989, vol. 37, pp. 2197–2210.
22. S. Li, I.J. Beyerlein, and M.A.M. Bourke: *Mater. Sci. Eng., A*, 2005, vol. 394, pp. 66–77.
23. S. Suwas, R. Arruffat-Massion, L.S. Tóth, A. Eberhardt, J.J. Fundenberger, and W. Skrotzki: *Metall. Mater. Trans. A* 2006, vol. 37A, pp. 739–53.
24. S. Suwas, B. Beausir, L.S. Tóth, J.J. Fundenberger, and G. Gottstein: *Acta Mater*., 2011, vol. 59, pp. 1121–33.
25. I.J. Beyerlein and L.S. Tóth: *Prog. Mater. Sci*., 2009, vol. 54, pp. 427–510.
26. HJ Bunge: *Texture Analysis in Materials Science: Mathematical Methods*, Butterworths, London, 1982.
27. Y. Beygelzimer, V. Varyukhin, S. Synkov, and D. Orlov: *Mater. Sci. Eng., A*, 2009, vol. 503, pp. 14–17.
28. S. Li, I.J. Beyerlein, C.T. Necker, D.J. Alexander, and M. Bourke: *Acta Mater*., 2004, vol. 52, pp. 4859–75.
29. I.J. Beyerlein, S. Li, C.T. Necker, D.J. Alexander, and C.N. Tomé: *Philos. Mag*., 2005, vol. 85, pp. 1359–94.
30. A.D. Rollett and S.I. Wright: in *Textures and Anisotropy. Preferred Orientations in Polycrystals and Their Effect on Materials Properties*, U.F. Kocks, C.N. Tome, and H.-R. Wenk, eds., Cambridge University Press, Cambridge, UK, 1998.
31. A.D. Rollett, T.C. Lowe, U.F. Kocks, and M.G. Stout: in *Eighth International Conference on Textures of Materials*, J.S. Kallend and G. Gottstein, eds., The Metallurgical Society, Warrendale, PA, 1988, pp. 437–478.
32. P.D. Wu, K.W. Neale, and E. Van der Giessen: *Int. J. Plast*., 1996, vol. 12, pp. 1199–219.
33. M. Berta, D. Orlov, and P.B. Prangnell: *Int. J. Mater. Res*., 2007, vol. 98, pp. 200–204.
34. H. Zendehdel and A. Hassani: *Mater. Des*., 2012, vol. 37, pp. 13–18.
35. S.R. Kalidindi, B.R. Donohue, and S. Li: *Int. J. Plast*., 2009, vol. 25, pp. 768–79.
36. Y. Beygelzimer, A. Reshetov, O. Prokof'eva, and R. Kulagin: *J. Mater. Process. Technol*., 2009, vol. 209, pp. 3650–56.
37. R. Kulagin, M.I. Latypov, H.S. Kim, V. Varyukhin, and Y. Beygelzimer: *Metall. Mater. Trans. A*, 2013, vol. 44A, pp. 3211–20.
38. L. Anand and S.R. Kalidindi: *Mech. Mater*., 1994, vol. 17, pp. 223–43.
39. Y.T. Zhu and T.C. Lowe: *Mater. Sci. Eng., A*, 2000, vol. 291, pp. 46–53.
40. L.S. Tóth, Y. Estrin, R. Lapovok, and C. Gu: *Acta Mater*., 2010, vol. 58, pp. 1782–94.
41. C.F. Gu and L.S. Tóth: *Acta Mater*., 2011, vol. 59, pp. 5749–57.
42. K. Kitayama, C.N. Tomé, E.F. Rauch, J.J. Gracio, and F. Barlat: *Int. J. Plast*., 2013, vol. 46, pp. 54–69.
43. M.-G. Lee, R.H. Wagoner, J.K. Lee, K. Chung, and H.Y. Kim: *Int. J. Plast*., 2008, vol. 24, pp. 545–82.